Biogeosciences Discuss., https://doi.org/10.5194/bg-2017-159
Manuscript under review for journal Biogeosciences
Discussion started: 1 June 2017

Biogeosciences Discussions Open Access EGU

Optical properties of size and chemical fractions of suspended particulate matter in littoral waters of Quebec

Gholamreza Mohammadpour[1], Jean-Pierre Gagné[1], Pierre Larouche[2], Martin A. Montes-Hugo[1*]

[1]Institut des Sciences de la Mer de Rimouski, 310 Alleé des Ursulines, Office P-216, Rimouski, Québec, Canada, G5L 3A1

[2]Institut Maurice-Lamontagne, Pêches et Océans Canada, Mont-Joli, Québec, Canada, G5H 3Z4

Correspondence to: Martin A. Montes-Hugo (martinalejandro_montes@uqar.ca)

Abstract. Mass-specific absorption (a_{SPM}^*) and scattering (b_{SPM}^*) coefficients of suspended particulate matter (SPM) were measured for different size (0.2-0.4 µm, 0.4-0.7 µm, 0.7-10 µm, and >10 µm) and chemical (organic- vs mineral-rich) fractions in surface waters (i.e., 0-5 m depth) of the Saint Lawrence Estuary and Saguenay Fjords (SLE-SF) during spring of 2013. For the spectral range 400-700 nm, scattering cross sections for particulate inorganic matter were commonly larger with respect to those measured in other littoral environments. This phenomenon was attributed the lower water turbidity and associated decrease on mean particle size of SLE-SF surface waters with respect to other river-influenced regions (e.g., Gironde River). a_{SPM}^* values in our study area were relatively high in locations having iron-enriched particulates. Lastly, correlation analysis suggests that particle composition (size distribution) has a larger impact on a_{SPM}^* (b_{SPM}^*) variability.

1 Introduction

The distribution of suspended particulate matter (SPM) in coastal and estuarine environments has a major influence on several biogeochemical processes (e.g., phytoplankton blooms) (Guinder et al., 2009), ecosystem structure (e.g., food webs) (Dalu et al., 2016) and dispersion of pollutants (e.g., copper, mercury, polycyclic aromatic hydrocarbons) (Ma et al., 2002; Ramalhosa et al., 2005; Tremblay et al., 2005). The concentration of SPM (C_{SPM}) is an important variable for estimating primary productivity (Devlin et al., 2008) and modeling thermodynamic processes (Löptien and Meier, 2011) due to its influence on underwater light attenuation (Morel and Antoine, 1994).

Remote sensing allows mapping of SPM in littoral environments where the spatial and temporal variability of suspended particulates is relatively high. Indeed, synoptic measurements derived from spaceborne ocean color sensors are commonly applied for estimating C_{SPM} based on visible (i.e., wavelength, λ = 400-700 nm) (Miller and McKnee, 2004; Montes-Hugo and Mohammadpour, 2012) and NIR-SWIR (near-and short-wave infrared) (λ = 700-3,000 nm) (Doxaran et al., 2002) spectral bands. Despite this progress, there is still a lack of understanding regarding how SPM microphysical characteristics (e.g., particle chemical composition and size distribution) relate to mass-specific inherent optical properties (IOPs). This

knowledge is essential for deriving more accurate remote sensing algorithms for estimating C_{SPM} and developing new optical inversions for retrieving second-order attributes of SPM (i.e., chemical composition, size distribution).

The remote sensing of particle size and/or composition in coastal and oceanic waters has been attempted based on four main methodologies: (1) analysis of spectral changes of IOPs (Loisel et al., 2006), (2) empirical relationships between mass-specific IOPs and biogeo-physical characteristics of SPM (e.g. mean diameter of particulates) (Bowers et al., 2009), (3) optical inversions of different volume scattering functions (Zhang et al., 2014), and (4) changes on water leaving polarized reflectance (Loisel et al., 2008).

The Saint Lawrence Estuary (SLE) and the Saguenay Fjords (SF) constitute a large sub-Arctic system characterized by relatively high concentrations of chromophoric dissolved organic matter (CDOM) (Nieke et al., 1997). The accurate monitoring of C_{SPM} and SPM characteristics in these waters is crucial for understanding regional climate effects on coastal erosion (Bernatchez and Dubois, 2004) and occurrence of harmful algae blooms (Fauchot et al. 2008). Despite this need, there is a lack of information regarding how optical properties are linked to particle second-order attributes and what is the spatial variability of mass-specific IOPs of SPM. For this reason, our contribution has two main objectives: (1) to characterize the mass-normalized IOPs for size and chemical fractions of SPM in different locations of the SLE-SF and during spring conditions, and (2) to establish relationships between mass-specific optical properties of SPM, 'bulk' particle characteristics related to size distribution and mineral content, and optical proxies within the visible and near-infrared spectral range (i.e., λ = 700-1,000 nm).

This study is organized in three sections. In the first section, mass-normalized spectral absorption and scattering coefficients for size and chemical SPM fractions are calculated for different optical environments of the SLE-SF that are characterized by a variable CDOM contribution to light attenuation and distinct particle assemblages. In the second section, the response of mass-normalized absorption and scattering coefficients of SPM fractions to variations in particle size distribution and mineral-content are investigated. Lastly in the third section, covariations between optical proxies and microphysical properties of SPM are examined.

2 Data and methods

2.1 Study area

The SLE can be divided in two main regions having contrasting biological productivity and bathymetry: the upper (UE) and the lower (LE) estuary (Levasseur et al., 1984). Non-algal particulates (NAP) and CDOM dominate the underwater light attenuation of UE waters (Nieke et al., 1997). This is in part related to the inflow of CDOM-rich and NAP-rich waters coming from the St. Lawrence River (Tremblay and Gagné, 2007). Unlike NAP and CDOM, contribution of phytoplankton to IOPs increases towards the mouth of the SLE (Montes-Hugo and Mohammadpour, 2012). Historical studies performed during summer of 1975 suggest that size distribution of SPM differs between UE, LE and SF regions (Poulet et al., 1986). Based on surface samples, Poulet et al. (1986) found a dominance of relatively 'small-sized' (i.e., mode diameter < 10 μm)

and 'large-sized' (i.e., > 30 µm) particulates over the UE and the mouth of the SLE, respectively. Conversely, the remaining locations of the LE were characterized by particulates having an intermediate size (i.e., 8-40 µm). In surface waters of SF, SPM is mainly composed by very small particles (i.e., 2-3 µm) during spring months (Chanut and Poulet, 1979). However, this pattern is reversed during autumn. Several investigations point out that suspended particulates in SLE-SF regions are principally composed by inorganic matter (D'Anglejan, and Smith, 1973; Larouche and Boyer-Villemaire, 2010). This mineral contribution varies between 60 and 95% of dry weight depending on location and period of the year (Yeats, 1988; Larouche and Boyer-Villemaire, 2010).

2.2 Field surveys

Discrete water samples for biogeochemical and optical measurements were obtained in 23 locations distributed throughout the SLE (n =18) and SF (n = 5) regions (Fig. 1). Samples corresponding to a sampling depth of 0-2 m were collected during June 3-9 of 2013 by using an oceanographic rosette equipped with Niskin bottles (volume = 12 L). For each sampling location, mass of different size fractions of SPM, IOPs for different SPM size fractions, and particle size distribution spectra were measured.

2.3 Biogeochemical analysis

The concentration of SPM and particulate inorganic matter (C_{PIM}) in g m^{-3} was measured gravimetrically with a precision of 15% and 25%, respectively (Mohammadpour et al., 2015). Size fractionation of SPM was done after sequentially filtering the original samples through pre-weighted membranes having a diameter of 47 mm and a pore size of 10 µm (Whatman, polycarbonate), 0.7 µm (GF/F, Whatman, glass fiber), 0.4 µm (Whatman, polycarbonate), and 0.2 µm (Nucleopore, polycarbonate). The contribution of size fraction i to the total mass of SPM (F_{SPM}^{i}, i = 0.2-0.4 µm, 0.4-0.7 µm, 0.7-10 µm, and >10 µm) was computed by normalizing their weight by the total weight of unfractioned samples that were retained on 0.2 µm membranes. The inorganic fraction of SPM (i.e., particulate inorganic matter or PIM) was obtained after removing the organic fraction (i.e., particulate organic matter or POM) of the original sample by combustion at 450°C for 6 h. Due to the dehydration of clays, this procedure may introduce an additional uncertainty of -10% and +10% on particulate inorganic (PIM) and organic matter (POM), respectively (Barillé-Boyer et al., 2003; Stavn et al., 2009). The contribution PIM and POM to SPM mass is F_{SPM}^{j} where j superscript symbolizes PIM or POM, respectively.

2.4 Optical measurements

Discrete water samples for CDOM absorption coefficient (a_{CDOM}) determinations were done in the lab following protocols suggested by Müller and Horn (1990). CDOM is defined here as the fraction or dissolved organic matter passing trough a membrane with a nominal pore size of 0.2 µm. Total absorption (a) and beam attenuation (c) coefficient measurements of four size-fractioned water samples (0.2 – 0.4 µm, 0.4 – 0.7 µm, 0.7 – 10 µm, and > 10 µm) were performed onboard using an absorption-beam attenuation meter (ac-s, WetLabs). Optical measurements were corrected by applying a flat baseline at a

Biogeosciences Discuss., https://doi.org/10.5194/bg-2017-159
Manuscript under review for journal Biogeosciences
Discussion started: 1 June 2017

reference wavelength of 715 nm (Bricaud and Stramski, 1990). This is a first order correction for scattering effects on non-water absorption coefficient estimates. Thus, the calculation of particulate absorption coefficients in this study is expected to have a bias with respect to true values measured using absorption-meter instruments that are less influenced by particulate scattering (e.g., point-source integrating-cavity absorption meters) (Röttgers et al., 2014). Spectral scattering coefficient measurements (b) were derived by subtracting a from c at each wavelength. The particle size spectra within the size range 3-170 µm were measured on 'bulk' (i.e., without size fractionation) samples and by using a red laser (wavelength = 670 nm) diffractometer (LISST-100X, type B, Sequoia Scientifics) (Agrawal et al. 1991).

2.5 Optical proxies of particle microphysical characteristics

Optical composite parameters directly related to remote sensing reflectance (R_{rs}) (Table 1) were constructed based on *in-water* IOPs determinations. Unfortunately, no remote sensing reflectance measurements were available during this study. Spectral values of a and b can be linked to the irradiance ratio measured just below the water surface ($R(0^-)$) (Morel and Prieur, 1977):

$$R(0^-) = f\ b\ b_b^{eff}/a \quad (1)$$

$$R_{rs} = R(0^-)\ \kappa/Q_n(\theta_0) \quad (2)$$

where f is a coefficient that varies with atmospheric (e.g., solar zenith angle) and water (e.g., single scattering albedo) parameters (Morel and Gentilli, 1996), b_b^{eff} is the total (i.e., water + particulates) backscattering efficiency (i.e., b_b/b) where b_b is the total backscattering coefficient). The magnitude of κ depends on refraction and internal reflection of photons at the air-water interface. For a nadir-looking sensor, the $Q_n(\theta_0)$is defined as the ratio between upwelling irradiance and upwelling radiance just beneath the sea surface and as a function of the solar zenith angle (θ_0). From equations (1) and (2), three biogeo-optical indices (BOI) were proposed for estimating changes in 'bulk' chemical composition (superscript comp) and size distribution (superscript size1 and size2) of SPM:

$$BOI^{comp} = a_{SPM}(\lambda_6)/a_{SPM}(\lambda_4) \quad (3)$$

$$BOI^{size1} = F((b(\lambda_1)\ a(\lambda_2))\ (a(\lambda_1)\ b(\lambda_2))^{-1}) \quad (4)$$

$$BOI^{size2} = F((b(\lambda_5)\ a(\lambda_3))\ (a(\lambda_5)\ b(\lambda_3))^{-1}) \quad (5)$$

where a_{SPM} is the particulate absorption coefficient, F is the polynomial function $g + g^2$, where $g = b(\lambda)\ (b(\lambda) + a(\lambda))^{-1}$. Notice that F resembles Gordon's formulation of R_{rs} for nadir-view geometry and optically deep water ($R_{rs} = \sum_{i=1}^{2} f_i\ (b_b\ (a + b_b)^{-1})^i$) (Gordon et al., 1988), where $f_1 \approx 0.0949$ I and $f_2 \approx 0.0794$ I, $I \approx t^2\ n^{-2}$ or the air-sea interface divergence factor (t is the air-sea transmittance and n is the refractive index of seawater). λ_1, λ_2, λ_3, λ_4, λ_5 and λ_6 correspond to wavelengths 443, 488, 555, 570, 670 and 675 nm, respectively. Values of a_{SPM} were derived by subtracting the contributions of CDOM and seawater to a. The absorption coefficient (a_w) and scattering (b_w) coefficient of seawater were computed at *in situ* salinity

Biogeosciences Discuss., https://doi.org/10.5194/bg-2017-159
Manuscript under review for journal Biogeosciences
Discussion started: 1 June 2017

and temperature by using empirical parameterizations suggested by Pope and Fry (1997) and Zhang et al. (2009), respectively.

The equation (3) was suggested based on empirical relationships between $a_{SPM}(\lambda_6)/a_{SPM}(\lambda_4)$ and POC/C_{SPM} ratios, where POC is the particulate organic carbon concentration (Wozniak et al., 2010). BOI^{size1} and BOI^{size2} indices for particle size distribution were based on Carder et al. (2004) and D'Sa et al. (2007) published R_{rs} band ratios, respectively. These ratios are correlated to the spectral slope of particulate backscattering. In general, BOI^{comp} values are expected to increase as SPM becomes richer in POC. Likewise, BOI^{size1} and BOI^{size2} are anticipated to decrease as particulates become larger or water contribution to backscattering increases at relatively low water turbidities.

2.6 Optical cross sections and mass-normalized IOPs

Spectral values of mass-specific absorption (σ_a^j) and scattering (σ_b^j) cross sections for mineral and organic fractions of SPM were estimated from multiple regression analysis (Sokal et al., 1995). The superscript j indicates inorganic (PIM) u organic (POM) particulate matter. For the case of size fractions of SPM, a mass-normalized optical property was calculated for particulate absorption and scattering coefficients:

$$a_i^*(\lambda) = a_i(\lambda)\,(m_i)^{-1} \quad (6)$$

$$b_i^*(\lambda) = b_i(\lambda)(m_i)^{-1} \quad (7)$$

where m is the mass in g m^{-3} for each size class i.

2.7 Statistical analysis

The influence of particle size and chemical composition variations on a_{SPM}, b_{SPM}, σ_a, σ_b, a_i^*, and b_i^* was investigated using the non-parametric Spearman rank correlation coefficient (ρ_s) (Spearman, 1904). This metrics was also applied to examine the response of a_i^* and b_i^* values to changes on the exponent of the power-law distribution of particle size distribution (γ) or the slope of log-transformed number of particulates per unit of volume as a function of their size range (Junge, 1963). Values of γ were computed based on linear regression models where dependent and independent variables are randomly selected (i.e., type II parameterization). Although particle size distribution in natural waters may not follow a Junge-type slope, its use here was justified since our main interest was to have a first-order assessment of size effects of particulates on IOPs variability. The sensitivity of BOI^{comp}, BOI^{size1}, and BOI^{size2} to variations of different chemical and SPM size fractions was quantified based on the magnitude of ρ_s. Lastly, potential functionalities between mass-normalized IOPs and BOI indices were examined for different study areas based on linear regression analysis model type II.

Biogeosciences Discuss., https://doi.org/10.5194/bg-2017-159
Manuscript under review for journal Biogeosciences
Discussion started: 1 June 2017

3 Results

3.1 Spatial variability of SPM fractions

In terms of particle size distribution, contrasting areas in the SLE-SF were identified. In UE, particulates having a diameter larger than 10 µm had in average a contribution of 11% to the total SPM mass (Table 2). This proportion was lower in the LE (up to 9%) and SF (up to 6%) sub-regions. The largest mass contribution of smallest-sized particulates (i.e., diameter < 0.4 µm) was calculated in the lower estuary. Lastly, the intermediate size class 0.7-10 µm was the fraction having the maximum contribution to SPM in the SF (76.5% in average). In general, the Junge slope calculations suggested the presence of relatively larger particulates in the LE with respect to UE and SF sub-regions. Indeed, the arithmetic average and range of γ for LE, UE and SF locations were 1.67 and 0.9-2.4, 2.4 and 2.3-2.4, and 2.4 and 2.1-2.6, respectively. The uncertainty of γ calculations varied between 8 and 90% with smaller errors in the LE. Unlike particle size distribution, chemical composition of SPM was less variable (F_{SPM}^{PIM} range = 20 - 87 %). In average for each sub-region under investigation, the mass of suspended particulates was always dominated by inorganic matter (arithmetic average of F_{SPM}^{PIM} = 0.58, 0.62 and 0.70 for SF, UE and LE, respectively, Table 2). The largest variability of mineral content of SPM was characteristic of waters with relatively shallow depths and a greater contribution of freshwater discharge by the St Lawrence River (e.g., sampling locations 12 and 13 in the UE, Fig. 1).

3.2 Relationships between SPM fractions and IOPs

In general, size and chemical composition of SPM were important second-order attributes affecting the scattering coefficient of suspended particulates. In general, b_{SPM} response to changes on SPM size fractions and chemical composition (ρ_s up to 0.71 and 0.59, t up to 21.17 and 15.35, Student-t test, respectively) was greater with respect to that associated to a_{SPM} (ρ_s up to 0.53 and 0.21, t up to 13.13 and 4.51, respectively, Student-t test) (Table 3). The larger influence of particle size distribution on b_{SPM} compared to a_{SPM} values was supported by correlations between γ and IOPs (ρ_s up to 0.50, t up to 12.12, Student-t test; ρ_s up to 0.33, t up to 7.34, Student-t test) (Table A1). Unlike particle size, the impact of SPM chemical composition on a_{SPM} was principally manifested at relatively short wavelengths (i.e., λ = 440-556 nm, ρ_s up to 0.21, t up to 4.51, Student-t test, Table 3). Indeed, the highest correlations between SPM size fractions and a_{SPM} values were computed in the red-NIR spectral regions (e.g., ρ_s up to 0.41, t up to 9.44, Student-t test).

3.3 Mass-specific optical properties of SPM

The variation of mass-normalized scattering and absorption coefficients of SPM for different size and chemical fractions are shown in Fig. 2. Full spectral variation of regional averaged a_{SPM}^* and b_{SPM}^* values are depicted in Fig. A1 (Appendix A). In general, sub-regional averages of mass-normalized IOPs of particulates with different size ranges were higher with respect to optical cross sections of chemical fractions (up to 2 and 3 orders of magnitude for a and b, respectively). For a wavelength of

Biogeosciences Discuss., https://doi.org/10.5194/bg-2017-159
Manuscript under review for journal Biogeosciences
Discussion started: 1 June 2017

556 nm and over the whole study area, the range of values for $a_{0.2\text{-}0.4\ \mu m}^{*}$, $a_{>10\ \mu m}^{*}$, σ_a^{PIM} and σ_a^{POM} was 0.11-2.14, 0.18-1.20, 0.01-1.06 and 0.01-1.03 $m^2\ g^{-1}$, respectively (Fig. 2a). Likewise, for the same wavelength, the range of $b_{0.2\text{-}0.4\ \mu m}^{*}$, $b_{>10\ \mu m}^{*}$, σ_b^{PIM} and σ_b^{POM} was 1.82-2.39, 1.05-1.49, 0.03-1.06 and 0.03-0.36 $m^2\ g^{-1}$, respectively (Fig. 2b).

For the spectral range 440-556 nm, mass-normalized absorption coefficients of SPM tended to be higher for particulates within the lower size range (i.e., 0.2-0.4 µm) (Fig. 2a, left-axis). Also, this trend appeared to be reversed at longer wavelengths. Unlike mass-normalized absorption coefficients of size fractions, mass-specific cross sections of chemical fractions showed only differences within the red and near-IR wavelengths (Fig. 2a, right-axis). For the whole study area, the arithmetic average of mass-normalized scattering coefficients for the size fraction 0.2-0.4 µm were larger with respect to that associated to the size fraction >10 µm (Fig. 2b, left-axis). At a wavelength of 440 nm, the mass-specific scattering cross sections for PIM were substantially higher (1.060 ± 0.206 $m^2\ g^{-1}$) than those corresponding to POM (0.359 ± 0.123 $m^2\ g^{-1}$) (Fig. 2b, right-axis).

In general, the magnitude of the mass-normalized absorption coefficient at 440 nm and computed for different size and chemical fractions was higher in UE-SF with respect to LE locations (Fig. 3a). Notice that absorption or scattering cross sections for chemical SPM fractions are not shown in UE locations given the insufficient number of samples to perform a multiple regression analysis. In Saguenay Fjord waters, the maximum $a_{SPM}^{*}(440)$ values (up to 4.6 $m^2\ g^{-1}$) were associated with the largest size fraction of SPM (Fig. 3, left-axis). Unlike size fractions, no substantial sub-regional differences were detected for $\sigma_a^{PIM}(440)$ and $\sigma_a^{POM}(440)$ values ($P > 0.05$, t up to 0.42, Student-t test) (Fig. 3, right-axis). In general, γ and F_{SPM}^{PIM} correlations with mass-normalized IOPs suggest that particle chemical composition has a larger influence on $a_i^{*}(440)$ (ρ_s up to 0.50, t up to 12.12, Student-t test) with respect to particle size (ρ_s up to 0.32, t up to 6.85, Student-t test) (Table 4). Unlike mass-specific absorption coefficients calculated at a wavelength of 440 nm, mass-specific scattering coefficients computed at 550 nm and for different size and chemical fractions of SPM presented smaller variations among spatial domains (Fig. 3b). Only for the intermediate size fraction 0.7-10 µm, the regional average of $b_i^{*}(550)$ in UE-SF (0.432-0.501 $m^2\ g^{-1}$) was larger with respect to that computed in LE waters (0.136 ± 0.027 $m^2\ g^{-1}$) (Fig. 3b, left-axis). Unlike $a_i^{*}(440)$, $b_i^{*}(550)$ variability was less influenced by changes on particle composition (ρ_s up to 0.42, t up to 9.72, Student-t test) (Table 4). Conversely, the impact of changing particle dimensions, as inferred from ρ_s correlations, was greater for $b_i^{*}(550)$ (ρ_s up to 0.37, t up to 8.36 Student-t test) with respect to $a_i^{*}(440)$ (ρ_s up to 0.33, t up to 7.34 Student-t test) values.

3.4 Optical proxies

Correlations between individual samples of size-based fractions of SPM and optical proxies of particle size and chemical composition are presented in Table 5. In general, it was found that BOI^{size1} was a more selective biogeo-optical indicator for retrieving second-order properties of SPM than BOI^{size2} and BOI^{comp}. Indeed, BOI^{size2} was also dependent on particle chemical composition variations as inferred from F_{SPM}^{PIM} ($\rho_s = -0.16$, $P < 0.05$, t = -3.40, Student-t test). Likewise, BOI_{comp} changes were also connected to variations of $F_{SPM}^{0.2\text{-}0.4\ \mu m}$ ($\rho_s = 0.34$, $t = 7.59$, Student-t test) and $F_{SPM}^{>10\ \mu m}$ ($\rho_s = -0.26$, t =

5.65, Student-t test) fractions. Despite these dependencies, BOI^{comp} had the strongest correlations with F_{SPM}^{PIM} values (ρ_s = 0.38, $P < 0.05$, t = 8.63, Student-t test). Optical proxies for estimating changes on particle size distributions had a different performance depending on the size fraction. Indeed, Carder et al. (2004) and D'Sa et al. (2007) indices were preferentially associated to changes of relatively small-sized (i.e., $F_{SPM}^{0.2\text{-}0.4\ \mu m}$, ρ_s up to -0.29, t up to -6.36, Student-t test) and intermediate-sized ($F_{SPM}^{0.4\text{-}0.7\ \mu m}$, ρ_s up to 0.35, t up to 7.85, Student-t test) particulates, respectively (Table 5). Unlike BOI^{comp}, BOI^{size1} and BOI^{size2} indices had a greater correlation with mass-specific IOPs and this dependency was stronger for larger particulates and mass-normalized absorption coefficients (ρ_s up to 0.74, t up 23.10 Student-t test). Since only three optical cross sections of SPM chemical fractions were computed over the whole study area, correlations between σ_a^j, σ_b^j, BOI^{size1}, BOI^{size2} and BOI^{comp} are not shown.

4 Discussion

4.1 Uncertainty of optical properties

Inherent optical properties in this study were derived from an ac-s instrument. Thus, large errors on absorption coefficients may be anticipated in relatively turbid waters if original measurements are not corrected by scattering effects (Boss et al., 2009; McKee et al., 2013). These effects are mainly attributed the acceptance angle of the transmissometer and the multiple scattering of photons. The acceptance angle of the ac-s instrument is ~0.9° and much larger than that corresponding to the LISST-100X diffractometer (~0.027°). Thus, a larger underestimation on c magnitude is expected in ac-s with respect to LISST-100X measurements due to a larger contribution of forward-scattered photons arriving to the detector of the former optical instrument. Further comparisons of $c(532)$ measurements derived here by ac-s and LISST-100X showed that c values as derived from ac-s were 23-84% lower with respect to those determinations based on LISST-100X. This is consistent with Boss et al. (2009) who reported that uncorrected Wet Labs ac-9 attenuation values are approximately 50%-80% of equivalent LISST attenuation data. Unfortunately, c deviations due to acceptance angle variations were not corrected in this study due to the lack of true c values as obtained by using an integrating cavity absorption meter (e.g., PSICAM) (Röttgers et al., 2005). Notice that these errors are much greater with respect to the optical variability associated to each sample determination as computed from ac-s measurements (e.g., < 1% at λ = 532 nm).

In this investigation, the 'flat' baseline correction was selected for correcting residual scattering in absorption coefficient estimates as derived from ac-s measurements. This technique was chosen due to the lack of PSICAM measurements or critical ancillary optical information (e.g., particle backscattering efficiency) to tune up a Monte Carlo scattering correction approach (McKee et al., 2008). The 'flat' scattering correction approach is expected to provide a fair correction of a values in oceanic waters (up to 15% underestimation at wavelengths shorter than 600 nm, see Fig. 8b, McKnee et al., 2013) but may result in large deviations (up to 100% decrease in the NIR) of a values in relatively turbid waters (e.g., $a > 0.2\ m^{-1}$) such as the Baltic/North Sea. Also, this issue is present when the proportional correction method of Zaneveld et al. (1994) is applied.

Unlike the 'flat' baseline, the scattering residual of the proportional method is spectrally dependent but still relying in one reference wavelength in the NIR spectral range. Approximations justifying the use of the 'flat' (i.e., zero absorption signal in the NIR) and 'proportional' (i.e., wavelength-dependent scattering phase function) method are still in debate (McKnee et al., 2013). Lastly, the Monte Carlo correction method (McKee et al., 2008) has in general better agreement (error <10%) with true a values as derived from an integrating cavity absorption meter. However, this approach may also have major uncertainties due to assumptions regarding IOPs (e.g., particulate backscattering ratio and volume scattering function) and changes on scattering efficiency by the inner wall of the reflective tube due to aging (McKnee et al., 2013). Thus in conclusion, the resulting particle-related IOPs and mass-specific optical coefficients obtained in the SLE-SF waters may present large errors (i.e., > 50%) with respect to true values and at wavelengths longer than 550 nm. This bias is anticipated to be maximum (minimum) in UE (LE) locations.

4.2 Spatial patterns of SPM microphysical characteristics

A striking finding in this study was the important weight contribution of relatively large particulates (i.e., >10 μm) in UE waters. This phenomenon was likely attributed to the active resuspension of sediments associated with vertical mixing produced by tidal currents and winds (Yeats, 1988). Conversely, this effect was secondary in relatively deep waters of SF and LE where large and heavy particulates are rapidly removed from the water column and deposited along submarine canyons (Gagné et al., 2009).

Although chemical composition of SPM size fractions was not analyzed in this study, additional correlations between total F_{SPM}^{PIM} and SPM size fractions values suggest that smallest particulates were richer in inorganic matter (ρ_s = 0.27, t up to 5.89, Student-t test, Table A2). Also, the opposite was true for the largest particulates (ρ_s = -0.27, t up to -5.89, Student-t test). This finding confirms previous studies showing that relatively small (~2 μm) particulates in the SLE are mainly composed by minerals (Yeats, 1988; Gagné et al., 2009).

In this contribution, a large proportion of particulates with a diameter above 50 μm and lower γ values were typically found in LE locations. This regional variation in SPM size distribution was attributed to the major influence of large-sized particulates derived from phytoplankton as γ was strongly correlated with chlorophyll a concentration (ρ_s = -0.45, t up to -10.58, Student-t test, Table A3). These results also support historical observations made during July and August and showing a greater proportion of relatively large particulates (i.e., > 5 and < 50 μm) over the LE locations (Chanut and Poulet, 1979).

4.3 Spatial variability of mass-specific optical coefficients

In this study, a_{SPM}^* measurements in the visible and near-IR range were in the upper range or higher than those reported in the literature for temperate coastal waters (e.g., Mobile Bay, River of La Plata, Elbe Estuary, Gironde Estuary) (Stavn and Richter, 2008; Doxaran et al., 2009; Dogliotti et al., 2015) (Table 6). In general, lowest a_{SPM}^* values commonly corresponded with samples obtained in very turbid environments (i.e., > 100 g m^{-3}, Gironde River, La Plata River) (Dogliotti

et al., 2015; Doxaran et al., 2009). Notice that part of this decrease can be attributed to an incomplete removal of multiple scattering effects. One mechanism explaining the general decrease of a_{SPM}^* in very turbid waters is related to packaging effects (Morel, 1974; Zhang et al., 2014). At higher turbidities, particulates become dominated by larger size distributions, thus as mean diameter of particles increases, the scattering efficiency of SPM decreases. In SF waters, the magnitude of $a_{>10\mu m}^*(440)$ values were higher with respect to those computed in other SLE sub-regions. These differences could be related to the relatively high concentrations of particulate iron in surface waters of the Saguenay Fjord (Yeats and Bewers, 1976; Tremblay and Gagné, 2009). Pigmentation of mineral particulate due to iron hydroxides has been suggested to be a major factor enhancing a_{SPM}^* (Babin and Stramski, 2004; Estapa et al., 2012).

Unlike a_{SPM}^*, the magnitude of b_{SPM}^* during our surveys was comparable, smaller or higher with respect to other studies depending on the wavelength and the type of environment. To exemplify, at the wavelength of 440 nm, the magnitude of our b_{SPM}^* measurements was comparable to that reported in coastal waters off Mississippi (Stavn and Richter, 2008). However, these values were higher compared to that reported in the Irish Sea waters (Bowers and Binding, 2006). The magnitude of σ_b^{POM} in our study area was relatively low with respect to those values reported in other littoral environments (e.g., Monterrey Bay, Mobile Bay and off New Jersey shore) (Snyder et al., 2008; Zhang et al., 2014).

4.4 Particle size and composition effects on mass-specific optical coefficients

Correlations of γ and F_{SPM}^{PIM} with mass-normalized IOPs for different SPM size fractions showed two contrasting optical responses (Table 4). First, γ was positively correlated with $a_i^*(440)$ (ρ_s up to 0.31, t up to 7.34, Student-t test) and $b_i^*(550)$ (ρ_s up to 0.37, t up to 14.19, Student-t test) for particulates larger than 10 μm. This pattern was due probably to the greater changes in particle density and associated variations on optical properties per unit of mass as particulates get bigger and more hydrated (Neukermans et al., 2012, Neukermans et al 2016; Reynolds et al., 2016). This effect is mainly observed in undisrupted marine aggregates (Slade et al. 2011). Since particle aggregates were altered during our experiments, this process is expected to be less important in explaining optical changes of suspended particulates. Based on theoretical calculations, Babin et al. (2003) showed a positive relationship between $b_{SPM}^*(550)$ and the differential Junge slope of particle size distribution. Also in this study, $b_{SPM}^*(550)$ was found to be directly related to γ (Table 4).

F_{SPM}^{PIM} had a stronger correlation with $a_i^*(440)$ compared with $b_i^*(550)$ values, and these relationships were stronger when SPM was dominated by particulates with an intermediate size (i.e., 0.4-10 μm). Babin et al. (2004) obtained positive correlations between a_{SPM}^* and iron content of minerals. In Arctic waters, Reynolds et al. (2016) observed an increase on mass-specific particulate backscattering for mineral-rich particle assemblages that tend to exhibit steeper size distributions. In summary, our results indicate that size (chemical composition) of suspended particulates has a major influence on spatial variability of b_i^* (a_i^*) in SLE-SF waters.

4.5 Optical proxies of particle size and composition

The response of three optical composite variables (BOI^{size1}, BOI^{size2} and BOI^{comp}) to changes on size and composition of different particle assemblages was evaluated based on correlation analysis. In general, BOI^{size1} was the most selective optical index for tracking variations on particle micro-physical properties. Indeed, BOI^{comp} (BOI^{size2}) was also substantially affected by size distribution (chemical composition) of SPM. The lack of specificity of BOI^{comp} may respond to the use of a spectral range where phytoplankton has a maximum light absorption peak (i.e., λ = 675 nm). As phytoplankton cells become larger (e.g., above 20 µm), the total chlorophyll a concentration of phytoplankton cells increases (Montes-Hugo et al., 2008). As result, the magnitude of a_{SPM} at a wavelength of 675 nm is expected to increase affecting positively BOI^{comp}. Lastly, BOI^{size1} and BOI^{size2} response was mainly associated with variability of small-sized and intermediate-sized SPM fractions, respectively. This selectivity is particularly interesting as both indexes may be combined for developing more robust metrics for estimating SPM size spectra distributions in littoral waters.

5 Conclusions

The measure of optical cross sections of SPM is essential for developing optical inversions and improve our understanding regarding the origin of optical signatures in remote sensing studies and map biogeo-chemical components in surface waters. In this contribution, we presented for the first time, mass-specific scattering and absorption coefficients of size fractioned SPM in estuarine waters of the Saint Lawrence River and a major SLE tributary, the Saguenay Fjord.

Despite the intrinsic variability of weight-normalized IOPs due to variations of particle micro-physical attributes, the following trends were observed: 1. the mass-specific absorption coefficient of SPM was preferentially influenced by changes in particle chemical composition, 2. particle size had a larger impact on b_{SPM}^{*} than a_{SPM}^{*}, and 3. optical proxies of SPM size distribution BOI^{size1} was more specific than optical proxy related to particle chemical composition (i.e., BOI^{comp}). These relationships are anticipated to be useful in the context of predicting mass-specific IOPs based on satellite remote sensing measurements.

6 Funding

This investigation was supported by the Natural Sciences and Engineering Research Council of Canada, Individual Discovery grant, project title: “Optical remote Sensing models of suspended Particulate matter in the St. Lawrence Estuary “(OSPLE), awarded to Dr. Martin Montes Hugo.

7 Acknowledgements

We thank to the crew of the Creed and Mr. Alexandre Palardy for their assistance during the field work. Also, we appreciate the support of ISMER technicians Mr. Pascal Rioux and Ms. Dominique Lavallée during the field surveys and the processing of lab measurements.

References

Agrawal, Y., McCave I. and Riley J.: Laser diffraction size analysis, in Principles, Methods, and Application of Particle Size Analysis, edited by James P. M. Syvitski, pp. 119–129, Cambridge University Press, N. Y., 1991.

Babin, M., Stramski D., Ferrari G.M., Claustre H., Bricaud, A., Obolensky, G. and Hoepffner N.: Variations in the light absorption coefficients of phytoplankton, nonalgal particles, and dissolved organic matter in coastal waters around Europe, J. Geophys. Res., 108, 10.1029/2001JC000882, 2003.

Babin, M. and Stramski, D.: Variations in the mass-specific absorption coefficient of mineral particles suspended in water, Limnol. Oceanogr., 49, 756–767, 2004.

Barillé-Boyer, A.L., Barillé, L., Massé, H., Razet, D. and Héral, M: Correction for particulate organic matter as estimated by loss on ignition in estuarine ecosystems, Estuar. Coast. Shelf Sci., 58, 147–153, 2003.

Bernatchez, P. and Dubois, J.-M. M.: Bilan des connaissances de la dynamique de l'érosion des côtes du Québec maritime laurentien, Géographie Phys. Quat., 58, 45, 2004 (in french).

Binding, C.E., Bowers, D.G. and Mitchelson-Jacob, E.G.: Estimating suspended sediment concentrations from ocean colour measurements in moderately turbid waters; the impact of variable particle scattering properties, Rem. Sens. Environ., 94, 373-383, 2005.

Boss, E., Slade, H., Behrenfeld, M. and Dall'Olmo, G.: Acceptance angle effects on the beam attenuation in the ocean, Opt. Expr., 17, 1535-1550, 2009.

Bowers, D. G. and Binding, C. E.: The optical properties of mineral suspended particles: A review and synthesis, Estuar. Coast. Shelf Sci., 67, 219–230, 2006.

Bowers, D.G., Braithwaite, K.M., Nimmo-Smith, W. A. M. and Graham, G. W.: Light scattering by particles suspended in the sea: The role of particle size and density, Cont. Shelf Res., 29, 1748–1755, 2009.

Bricaud, A. and Stramski, D.: Spectral absorption coefficients of living phytoplankton and nonalgal biogenous matter: Aa comparison between Peru upwelling area and the Sargasso Sea, Limnol. Oceanogr., 35, 562-582, 1990.

Carder, K. L., Chen, F. R., Cannizzaro, J. P., Campbell, J. W., and Mitchell, B. G.: Performance of the MODIS semi-analytical ocean color algorithm for chlorophyll-a, Adv. Sp. Res., 33, 1152–1159, 2004.

Chanut, J. P. and Poulet, S. A.: Short-term variability of the size spectra of suspended particles in a rapidly changing environment., Estuar. Coast. Shelf Sci., 15, 497–513, 1982.

D'Anglejan, B. F. and Smith, E. C.: Distribution, Transport, and Composition of Suspended Matter in the St. Lawrence Estuary, Can. J. Earth Sci., 10, 1380–1396, 1973.

Dalu, T., Richoux, N. B., and Froneman, P. W.: Nature and source of suspended particulate matter and detritus along an austral temperate river-estuary continuum, assessed using stable isotope analysis, Hydrobiologia, 767, 95-110, 2016.

Devlin, M. J., Barry, J., Mills, D. K., Gowen, R. J., Foden, J., Sivyer, D., and Tett, P.: Relationships between suspended particulate material, light attenuation and Secchi depth in UK marine waters, Estuar. Coast. Res. Shelf Sci., 79, 429-439, 2008.

D'Sa, E. J., Miller, R. L. and McKee, B. A.: Suspended particulate matter dynamics in coastal waters from ocean color: Application to the northern Gulf of Mexico, Geophys. Res. Lett., 34, 1–6, 2007.

Dogliotti, A. I., Ruddick, K. G., Nechad, B., Doxaran, D. and Knaeps, E.: A single algorithm to retrieve turbidity from remotely-sensed data in all coastal and estuarine waters, Remote Sens. Environ., 156, 157–168, 2015.

Doxaran, D., Froidefond, J. M., Lavender, S., and Castaing, P.: Spectral signature of highly turbid waters: Application with SPOT data to quantify suspended particulate matter concentrations, Remote Sens. Environ., 81, 149–161, 2002.

Doxaran, D., Ruddick, K., McKee, D., Gentili, B., Tailliez, D., Chami, M. and Babin, M.: Spectral variation of light scattering by marine paticles in coastal waters, from visible to near infrared, Limnol. Oceanogr., 54, 1257–1271, , 2009.

Estapa, M. L., Boss, E., Mayer, L. M. and Roesler, C. S.: Role of iron and organic carbon in mass-specific light absorption by particulate matter from Louisiana coastal waters, Limnol. Oceanogr., 57, 97–112, 2012.

Fauchot, J., Saucier, F. J., Levasseur, M., Roy, S. and Zakardjian, B.: Wind-driven river plume dynamics and toxic Alexandrium tamarense blooms in the St. Lawrence estuary (Canada): A modeling study, Harmful Algae, 7, 214–227, 2008.

Gagné, H., Lajeunesse, P., St-Onge, G. and Bolduc, A.: Recent transfer of coastal sediments to the Laurentian Channel, Lower St. Lawrence Estuary (Eastern Canada), through submarine canyon and fan systems, Geo-Marine Lett., 29, 191–200, 2009.

Gordon, H.R., Brown, O.B., Evans, R.H., Brown, J.W., Smith, R.C., Baker, K.S., Clark, D.K., A semi-analytic radiance model of ocean color, J. Geophys. Res., 93, 10909-10924, 1988.

Guinder, V. A., Popovich, C. A., and Perillo, G. M. E.: Particulate suspended matter concentrations in the Bahia Blanca Estuary, Argentina: Implication for the development of phytoplankton blooms, Estuar. Coast. Res. Shelf Sci., 85, 157-165, 2009.

Junge, C. E.: Air chemistry and radioactivity, Acad. Press INC, 11, 1253, , 1963.

Larouche, P. and Boyer-Villemaire, U.: Suspended particulate matter in the St. Lawrence estuary and Gulf surface layer and development of a remote sensing algorithm, Estuar. Coast. Shelf Sci., 90, 241–249, 2010.

Levasseur, M., Therriault, J.-C. and Legendre, L.: Hierarchical control of phytoplankton succession by physical factors, Mar. Ecol. Prog. Ser., 19, 211–222, 1984.

Loisel, H., Nicolas, J. M., Sciandra, A., Stramski, D. and Poteau, A.: Spectral dependency of optical backscattering by marine particles from satellite remote sensing of the global ocean, J. Geophys. Res. Ocean., 111, 1–14, 2006.

Loisel, H., Duforet, L., Dessailly, D., Chami, M., and Dubuisson, P.: Investigation of the variations in the water leaving polarized reflectance from the POLDER satellite data over two biogeochemical contrasted oceanic areas, Opt. Exp., 17, 12905-12918, 2008.

Löptien, U. and Meier, H. E. M.: The influence of increasing water turbidity on the sea surface temperature in the Baltic Sea: A model sensitivity study, J. Mar. Syst., 88, 323–331, 2011.

Ma, H., Kim, S. D., Allen, H. E., and Cha, D. K.: Effect of copper binding by suspended particulate matter on toxicity, Environ. Toxicol. Chem. 21, 710-714, 2002.

McKee, D., Piskozub, J. and Brown, I. 2008: Scattering error corrections for in situ absorption and attenuation measurements, Opt. Exp., 16, 19480-19492.

McKee, D., Piskozub, J., Röttgers, R., Reynolds, R.A.: Evaluation and improvement of an iterative scattering correction scheme for in situ absorption and attenuation measurements, J.Amer. Ocean. Technol.,30, doi.10.1175/JTECH-D-12-00150.1, 2013.

Miller, R. L. and McKee, B. A.: Using MODIS Terra 250 m imagery to map concentrations of total suspended matter in coastal waters, Remote Sens. Environ., 93, 259–266, 2004.

Mohammadpour, G., Montes-Hugo, M. A., Stavn, R., Gagné, J. P. and Larouche, P.: Particle Composition Effects on MERIS-Derived SPM: A Case Study in the Saint Lawrence Estuary, Can. J. Remote Sens., 41, 515–524, 2015.

Montes-Hugo, M., Vernet, M., Martinson, D., Smith, R. and Iannuzzi, R.: Variability on phytoplankton size structure in the western Antarctic Peninsula (1997–2006), Deep Sea Res. Part II Top. Stud. Oceanogr., 55, 2106–2117, 2008.

Montes-Hugo, M. A. and Mohammadpour, G.: Biogeo-optical modeling of SPM in the St. Lawrence Estuary, Can. J. Remote Sens., 38, 197–209, 2012.

Morel, A.: Optical properties of pure water and pure seawater, p.1-24,In. N.G. Jerlov and E. Steemann Nielsen (eds.), Optical aspects of oceanography Academic, 1974.

Morel, A. and Antoine, D.: Heating Rate within the Upper Ocean in Relation to its Bio–optical State, J. Phys. Oceanogr., 24, 1652–1665, 1994.

Morel, A. and Prieur, L.: Analysis of variations in ocean color, Limnol. Oceanogr., 22, 709–722, 1977.

Morel, A. and Gentili, B.: Diffuse reflectance of oceanic waters. III. Implication of bidirectionality for the remote-sensing problem., Appl. Opt., 35, 4850–4862, 1996.

Müller HW. and Horn K., Some Technical Aspects of a High Quality UV/Vis Spectrometer for Routine Analysis, Applied UV Spectroscopy 19D, Bodenseewerk Perkin-Elmer GmbH, Überlingen, 1990.

Neukermans, G., Loisel, H., Mériaux, X., Astoreca, R. and McKee, D.: In situ variability of mass-specific beam attenuation and backscattering of marine particles with respect to particle size, density, and composition, Limnol. Oceanogr., 57, 124–144, 2012.

Neukermans, G., Reynolds, R. A. and Stramski, D.: Optical classification and characterization of marine particle assemblages within the western Arctic Ocean, Limnol. Oceanogr., 61, 1472–1494, 2016.

Nieke, B., Reuter, R., Heuermann, R., Wang, H., Babin, M. and Therriault, J. C.: Light absorption and fluorescence properties of chromophoric dissolved organic matter (CDOM), in the St. Lawrence Estuary (Case 2 waters), Cont. Shelf Res., 17, 235–252, 1997.

Pope, R. M. and Fry, E. S.: Absorption spectrum (380-700nm) of pure water. II . Integrating cavity measurements, Appl. Opt., 36, 8710–8723, 1997.

Poulet, S., Cossa, D. and Marty, J.-C.: Combined analyses of the size spectra and biochemical composition of particles in the St. Lawrence estuary, Mar. Ecol. Prog. Ser., 30, 205–214, 1986.

Ramalhosa, E., Pereira, E., Vale, C., Válega, M., Monterroso, and P., Duarte, A. C.: Mercury distribution in Douro estuary (Portugal), Mar. Poll. Bull. 50, 1218-1222, 2005.

Reynolds, R. A., Stramski, D. and Neukermans, G.: Optical backscattering by particles in Arctic seawater and relationships to particle mass concentration, size distribution, and bulk composition, Limnol. Oceanogr., 61, 1869–1890, 2016.

Röttgers, R., Schönfeld, W., Kipp, P.R., Doerffer, R.: Practical test of a point-source integrating cavity absorption meter: The performance of different collector assemblies, App. Opt., 44, 5549-5560, 2005.

Röttgers, R., McKee, D., and Woźniak, S. B.: Evaluation of scatter corrections for ac-9 absorption measurements in coastal waters, Methods Oceanogr., 7, 21–39, 2013.

Röttgers, R., Dupouy, C., Taylor, B. B., Bracher, A. and Woźniak, S. B.: Mass-specific light absorption coefficients of natural aquatic particles in the near-infrared spectral region, Limnol. Oceanogr., 59, 1449–1460, 2014.

Slade, W.H., Boss, E. and Russo C.: Effects of particle aggregation and disaggregation on their inherent optical properties, Opt. Exp., 19, 7945-7959, 2011.

Snyder, W., Arnone, R., Davis, C. O., Goode, W., Gould, R. W., Ladner, S., Lamela, G., Rhea, W. J., Stavn, R., Sydor, M. and Weidemann, A.: Optical scattering and backscattering by organic and inorganic particulates in U.S. coastal waters., Appl. Opt., 47, 666–77, 2008.

Sokal, R. R. and Rohlf, F. J.: Biometry: the principles of statistics in biological research, 3rd ed., WH Freeman and Co, New York, NY., 1995.

Spearman, C.: The Proof and Measurement of Association between two things, The Amer. J. of Psych. , 15 , 1904.

Stavn, R. H. and Richter, S. J.: Biogeo-optics: particle optical properties and the partitioning of the spectral scattering coefficient of ocean waters., Appl. Opt., 47, 2660–2679, 2008.

Stavn, R.H., Rick H.J., and Falster and A.V.:Correcting the errors from variable sea salt retention and water of hydration in loss on ignition analysis: Implications for studies of estuarine and coastal waters, Estuar. Coast. Shelf Sci., 81, 575-582, 2009.

Tremblay, L. and Gagné, J. P.: Distribution and biogeochemistry of sedimentary humic substances in the St. Lawrence Estuary and the Saguenay Fjord, Québec, Org. Geochem., 38, 682–699, 2007.

Tremblay, L. and Gagné, J. P.: Organic matter distribution and reactivity in the waters of a large estuarine system, Mar. Chem., 116, 1–12, 2009.

Tremblay, L., Kohl, S. D., Rice, J. A. and Gagné, J. -P.: Effects of temperature, salinity, and dissolved humic substances on the sorption of polycyclic aromatic hydrocarbons to estuarine particles, Mar. Chem., 96, 21–34, 2005.

Woźniak, S. B., Stramski, D., Stramska, M., Reynolds, R. A., Wright, V. M., Miksic, E. Y., Cichocka, M. and Cieplak, A. M.: Optical variability of seawater in relation to particle concentration, composition, and size distribution in the nearshore marine environment at Imperial Beach, California, J. Geophys. Res. Ocean., 115, 1–19, 2010.

Xi, H., Larouche, P., Tang, S. and Michel, C.: Seasonal variability of light absorption properties and water optical constituents in Hudson Bay, Canada, J. Geophys. Res. Ocean., 118, 3087–3102, 2013.

Yeats, P. A.: The distribution of trace metals in ocean waters, Sci. Total Environ., 72, 131–149, 1988.

Yeats, P. A. and Bewers, J. M.: Trace metals in the waters of the Saguenay Fjord, Can. J. Earth Sci., 13, 1319–1327, 1976.

Zaneveld, J.R.V., Kitchen, J.C., Moore, C.M.: The scattering correction error of the reflecting-tube absorption meters, Ocean Optics XII, J.S. Jaffe, Ed. International Society for Optical Engineering, SPIE proceedings, vol. 2258, 44-58, 1994.

Zhang, X., Hu, L., and He, M.-X.: Scattering by pure seawater: Effect of salinity, Opt. Exp., 17, 5698–5710, 2009.

Zhang, X., Stavn, R. H., Falster, A. U., Gray, D. and Gould, R. W.: New insight into particulate mineral and organic matter in coastal ocean waters through optical inversion, Estuar. Coast. Res. Shelf Sci., 149, 1–12, 2014.

Biogeosciences Discuss., https://doi.org/10.5194/bg-2017-159
Manuscript under review for journal Biogeosciences
Discussion started: 1 June 2017

Table 1. Summary of acronyms

Abbreviation	Definition	Unit
SLE	St. Lawrence Estuary	
UE	Upper Estuary	
SF	Saguenay Fjord	
LE	Lower Estuary	
C_{SPM}	Concentration of suspended particulate matter	g m^{-3}
F_{SPM}^{i}	Contribution of size fraction i to total mass of SPM	dimensionless
F_{SPM}^{j}	Contribution of chemical fraction j to total mass of SPM	dimensionless
NAP	Non-algal particulates	
CDOM	Chromophoric dissolved organic matter	
PIM	Particulate inorganic matter	g m^{-3}
POM	Particulate organic matter	g m^{-3}
λ	Light wavelength	nm
a_{SPM}	Absorption coefficient of SPM	m^{-1}
b_{SPM}	Scattering coefficient of SPM	m^{-1}
a_{SPM}^{*}	Mass-specific absorption coefficient of SPM	m^2 g^{-1}
b_{SPM}^{*}	Mass-specific scattering coefficient of SPM	m^2 g^{-1}
σ_a^j	Absorption cross section of SPM chemical fraction j	m^2 g^{-1}
σ_b^j	Scattering cross section of SPM chemical fraction j	m^2 g^{-1}

b_b^{eff}	Backscattering efficiency	dimensionless
γ	Differential Junge slope	Number of particulates per µm
BOI^{size}	Biogeo-optical proxy for size distribution of SPM	dimensionless
BOI^{comp}	Biogeo-optical proxy for chemical composition of SPM	dimensionless

Biogeosciences Discuss., https://doi.org/10.5194/bg-2017-159
Manuscript under review for journal Biogeosciences
Discussion started: 1 June 2017

Table 2. Summary of biogeochemical variables during June 2013. Acronyms UE, SF, LE are defined in Table 1. N is the number of samples per sub-region.

Sub-region	Fraction	Range	N
UE	F_{SPM}^{PIM}	0.37 – 0.87	3
	$F_{SPM}^{0.2-0.4\ \mu m}$	0.04-0.08	3
	$F_{SPM}^{0.4-0.7\ \mu m}$	0.01-0.04	3
	$F_{SPM}^{0.7-10\ \mu m}$	0.77-0.89	3
	$F_{SPM}^{>10\ \mu m}$	0.05-0.17	3
SF	F_{SPM}^{PIM}	0.49 – 0.66	5
	$F_{SPM}^{0.2-0.4\ \mu m}$	0.05-0.11	5
	$F_{SPM}^{0.4-0.7\ \mu m}$	0.01-0.14	5
	$F_{SPM}^{0.7-10\ \mu m}$	0.66-0.87	5
	$F_{SPM}^{>10\ \mu m}$	0.01-0.11	5
LE	F_{SPM}^{PIM}	0.53 – 0.87	15
	$F_{SPM}^{0.2-0.4\ \mu m}$	0.02-0.27	15
	$F_{SPM}^{0.4-0.7\ \mu m}$	0.01-0.10	15
	$F_{SPM}^{0.7-10\ \mu m}$	0.48-0.93	15
	$F_{SPM}^{>10\ \mu m}$	0.03-0.15	15

Biogeosciences Discuss., https://doi.org/10.5194/bg-2017-159
Manuscript under review for journal Biogeosciences
Discussion started: 1 June 2017

Table 3. Correlation between IOPs of suspended particulates and SPM mass fractions. Each value is ρ_s with a statistical confidence level at 95 and 99% is symbolized with * and **, respectively. The number of observations per correlation is 23.

	λ	a_{SPM}	b_{SPM}
F_{SPM}^{PIM}	440	0.21 **	0.59**
	556	0.12 *	0.58**
	665	0.02	0.56 **
	708	0.17 *	0.55 **
$F_{SPM}^{0.2\text{-}0.4\ \mu m}$	440	-0.01	0.66 **
	556	0.03	0.71 **
	665	-0.03	0.70 **
	708	-0.13 *	0.66 **
$F_{SPM}^{0.4\text{-}0.7\ \mu m}$	440	-0.06	0.28 **
	556	-0.05	0.35 **
	665	-0.09	0.31 **
	708	-0.20 **	0.27 **
$F_{SPM}^{0.7\text{-}10\ \mu m}$	440	-0.12 *	-0.65 **
	556	-0.14 *	-0.67 **
	665	-0.17 *	-0.63**
	708	-0.03	-0.57 **
$F_{SPM}^{>10\ \mu m}$	440	0.36 **	0.47 **
	556	0.35 *	0.39 **
	665	0.53 **	0.33 **
	708	0.41 **	0.28 **

5

Table 4. Particle size and chemical composition effects on mass-normalized IOPs. Spearman rank correlations for a_i^* and b_i^* are computed at a wavelength of 440 and 550 nm, respectively.

γ	F_{SPM}^{PIM}

Biogeosciences Discuss., https://doi.org/10.5194/bg-2017-159
Manuscript under review for journal Biogeosciences
Discussion started: 1 June 2017

$a_{0.2-0.4\ \mu m}^{*}$	0.32 **	0.31 **
$a_{0.4-0.7\ \mu m}^{*}$	0.28 **	0.50 **
$a_{0.7-10\ \mu m}^{*}$	0.26 **	0.49 **
$a_{>10\ \mu m}^{*}$	0.31 **	0.44 **
$b_{0.2-0.4\ \mu m}^{*}$	0.15 *	-0.17 *
$b_{0.4-0.7\ \mu m}^{*}$	0.05	-0.06
$b_{0.7-10\ \mu m}^{*}$	0.23 **	0.42 **
$b_{>10\ \mu m}^{*}$	0.37 **	0.26 **

Table 5. Particle size and chemical composition effects on optical proxies. Statistic confidence levels of ρ_s values are described in Table 3.

	BOI^{size1}	BOI^{size2}	BOI^{comp}

Biogeosciences Discuss., https://doi.org/10.5194/bg-2017-159
Manuscript under review for journal Biogeosciences
Discussion started: 1 June 2017

F_{SPM}^{PIM}	-0.02	-0.16 *	0.38 **
$F_{SPM}^{0.2\text{-}0.4\ \mu m}$	-0.29 **	0.03	0.34 **
$F_{SPM}^{0.4\text{-}0.7\ \mu m}$	-0.28**	0.35**	-0.20**
$F_{SPM}^{0.7\text{-}10\ \mu m}$	0.27**	-0.12*	-0.21*
$F_{SPM}^{>10\ \mu m}$	-0.01	-0.10	0.26*

Table 6. Mass-normalized optical coefficients of suspended particulates for different littoral environments. Acronyms are defined in Table 1.

Biogeosciences Discuss., https://doi.org/10.5194/bg-2017-159
Manuscript under review for journal Biogeosciences
Discussion started: 1 June 2017

Location	λ	a_{SPM}^{*}	b_{SPM}^{*}	σ_a^{POM}	σ_a^{PIM}	σ_b^{POM}	σ_b^{PIM}	C_{SPM}	References
UE	440	0.01 – 2.68	0.01 – 2.71	0.15	0.11	0.84	2.27	7.38 – 30.6	This study
	488	0.01 – 0.99	0.01 – 2.70	0.06	0.05	0.76	2.04		
	556	0.01 – 0.32	0.01 – 2.55	0.01	0.01	0.71	1.82		
	665	0.01 – 0.15	0.01 – 1.75	0.01	0.05	0.45	1.67		
	708	0.01 – 0.12	0.01 – 0.79	0.01	0.02	0.11	1.31		
SF	440	0.01 – 2.61	0.03 – 2.39	1.71	0.86	1.78	0.94	2.28 – 3.68	
	488	0.01 – 1.76	0.05 – 1.76	1.84	0.43	1.14	0.88		
	556	0.01 – 1.55	0.05 – 1.68	0.85	0.17	0.45	0.56		
	665	0.01 – 0.70	0.01 – 0.68	0.12	0.11	0.23	0.12		
	708	0.01 – 0.44	0.01 – 0.49	0.01	0.01	0.12	0.04		
LE	440	0.01 – 1.95	0.01 – 2.17	0.07	0.02	2.64	2.04	2.72 – 25.7	
	488	0.01 – 1.24	0.01 – 2.06	0.03	0.01	2.13	1.88		
	556	0.01 – 1.18	0.01 – 1.38	0.01	0.01	1.88	1.36		
	665	0.01 – 1.04	0.01 – 1.03	0.02	0.01	1.42	0.89		
	708	0.01 – 0.88	0.01 – 0.88	0.02	0.01	0.98	0.67		
Elber River,	650	0.001 – 0.020						0.5-10	Röttgers et al. (2014)

German Bight,	750	0.001 – 0.019					
Baltic Sea, New Caledonia lagoon	850	0.001 – 0.014					
Monterey Bay, US	532		0.46 – 2.54	1.23–3.39	0.08 – 0.77	0.11 – 2.37	Zhang et al. (2014)
Mobile Bay, US	532		0.40 – 1.78	0.35–3.85	0.27 – 0.79	0.26 – 7.36	
Hudson Bay, Canada	675	0.001 – 0.12				0.2 – 2.5	Xi et al. (2013)
Mississippi River, US	450	0.02 – 0.11				7-25	Bowers and Binding (2006)
	550	0.017 – 0.06					
	650	0.012–0.035					
	700	0.01 – 0.025					
Mobile Bay,	440	0.44 – 1.95		0.01-1.91	0.36 – 0.80	0.23-25.32	Stavn and Richter

Biogeosciences Discuss., https://doi.org/10.5194/bg-2017-159
Manuscript under review for journal Biogeosciences
Discussion started: 1 June 2017

								(2008)
Southwest Pass, US	488	0.41 – 1.89			0.01-1.82	0.36-0.73		
	550	0.40 – 1.80			0.01-1.65	0.33-0.70		
	676	0.36 – 1.63			0.04-1.48	0.34-0.63		
	715	0.34 – 1.61			0.02-1.39	0.33-0.58		
Coast of New Jersey,	440		0.23 – 0.59	0.08– 0.17	0.7 – 5.1	0.3 – 1.3	0.44 – 6.6	Snyder et al. (2008)
Monterey Bay,	488		0.18 – 0.39	0.07– 0.13	0.65 – 4.8	0.4 – 1.6		
Great Bay	556		0.13 – 0.21	0.05– 0.08	0.4 – 4.3	0.5 – 1.8		
	665		0.09 – 0.11	0.05– 0.06	0.35 – 3.8	0.4 – 1.7		
	708		0.02 – 0.03	0.01– 0.02	0.4-3.9	0.3-1.7		
Irish sea, UK	665	0.08 – 0.45		0.01 – 0.02		0.47 – 0.49	1.9 – 26.5	Binding et al. (2005)
Irish sea, UK	443	0.17 – 0.19		0.05 – 0.06		0.25 – 0.27	1.6 – 50	Bowers and Binding (2006)

	490		0.20 – 0.22	0.03 – 0.04	0.33 – 0.37	
	555		0.20 – 0.24	0.03 – 0.03	0.37 – 0.39	
	665		0.14 – 0.15	0.02 – 0.03	0.27 – 0.29	
English channel, UK	550		0.62 – 1.04		0.01 – 72.8	
Coast off Europe and French Guyana	676		0.63 – 2.07		0.12 – 1.83	1.2 – 82.4	Neukermans et al. (2012)
Guyana coast, Scheldt River, Gironde River, Rio de la Plata Estuary	440	0.02 – 0.12			0.37 – 0.89	30 – 120	Dogliotti et al. (2015)
Elbe Estuary,	555	0.05 – 0.07	0.35 – 0.47			73.5 – 294.2	Doxaran et al. (2009)

Germany				
	715	0.01 – 0.03	0.32 – 0.44	
Gironde Estuary, France	555	0.02 – 0.06	0.28 – 0.50	21.9 – 344.1
	715	0.01 – 0.02	0.27 – 0.45	

Biogeosciences Discuss., https://doi.org/10.5194/bg-2017-159
Manuscript under review for journal Biogeosciences
Discussion started: 1 June 2017

Appendix A

Table A1. Correlations between γ, F_{SPM}^{PIM}, and IOPs of SPM size fractions. First, second, third and fourth ρ_s values correspond to the wavelengths 440, 556, 665 and 708 nm, respectively.

	γ	F_{SPM}^{PIM}
$a_{0.2\text{-}0.4\ \mu m}$	-0.17*, 0.21**, 0.01,0.01	0.10*,0.29**,0.12*,0.12*
$a_{0.4\text{-}0.7\ \mu m}$	0.31**,0.07,0.33**,0.20*	0.62**,-0.17*,0.35**,0.36**
$a_{0.7\text{-}10\ \mu m}$	0.07,0.31**,0.07,0.11*	-0.17*,0.62**,-0.02,0.01
$a_{>10\ \mu m}$	0.21**,0.30**,-0.30**,0.08	0.29**,0.42**,0.15*,0.01
$b_{0.2\text{-}0.4\ \mu m}$	-0.29**,0.26**,-0.30**,-0.25**	-0.03,0.16*,0.15*,0.19*
$b_{0.4\text{-}0.7\ \mu m}$	-0.21**,0.18*,-0.21**,-0.16*	-0.15*,0.28**,-0.10,-0.06
$b_{0.7\text{-}10\ \mu m}$	0.50*,0.16*,0.50**,0.41**	0.28**,0.01,0.16*,0.17*
$b_{>10\ \mu m}$	0.34**,0.05,0.24**,0.19*	0.59**,-0.13*,0.52**,0.44**

Biogeosciences Discuss., https://doi.org/10.5194/bg-2017-159
Manuscript under review for journal Biogeosciences
Discussion started: 1 June 2017

Table A2. Correlations between size and chemical fractions of SPM.

	F_{SPM}^{PIM}
$F_{SPM}^{0.2-0.4\ \mu m}$	0.27 **
$F_{SPM}^{0.4-0.7\ \mu m}$	0.15 *
$F_{SPM}^{0.7-10\ \mu m}$	0.08
$F_{SPM}^{>10\ \mu m}$	-0.27 **

Biogeosciences Discuss., https://doi.org/10.5194/bg-2017-159
Manuscript under review for journal Biogeosciences
Discussion started: 1 June 2017

Table A3. Correlations between chlorophyll a concentration and γ. N is the number of observations.

	γ	N
UE	-0.08	3
SF	0.62 **	4
LE	-0.45 **	14

Biogeosciences Discuss., https://doi.org/10.5194/bg-2017-159
Manuscript under review for journal Biogeosciences
Discussion started: 1 June 2017

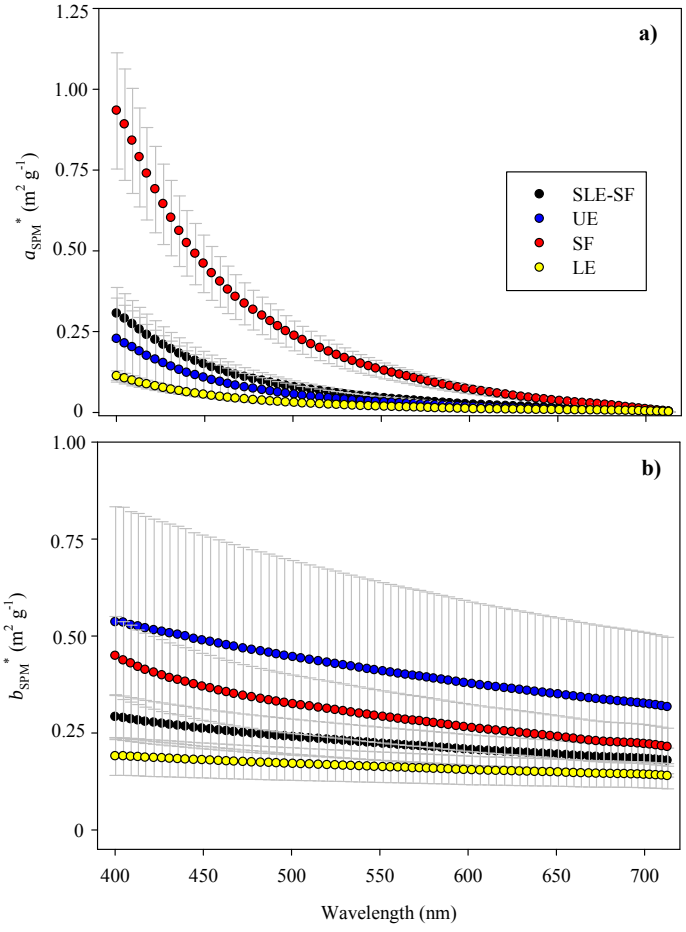

fig A1

5

Biogeosciences Discuss., https://doi.org/10.5194/bg-2017-159
Manuscript under review for journal Biogeosciences
Discussion started: 1 June 2017

Figure captions

Figure 1. Study area. UE (green triangles), LE (blue rectangles) and SF (red circles). GSL is the Gulf of St. Lawrence.

Figure 2. Spectral variation of mass-normalized optical coefficients of SPM. (a) particulate absorption at λ = 440 nm, (b) particulate scattering at λ = 550 nm. Each bar corresponds to the arithmetic average over the whole study area; uncertainty bars symbolize ± 2 standard errors.

Figure 3. Sub-regional variation of mass-normalized optical coefficients of SPM. (a) particulate absorption at λ = 440 nm, (b) particulate scattering at λ = 550 nm.

Figure A1. Spectral variation of mass-specific absorption and scattering coefficients of suspended particulate matter. (a) absorption, (b) scattering. Error bars represent 1 standard error.

Biogeosciences Discuss., https://doi.org/10.5194/bg-2017-159
Manuscript under review for journal Biogeosciences
Discussion started: 1 June 2017

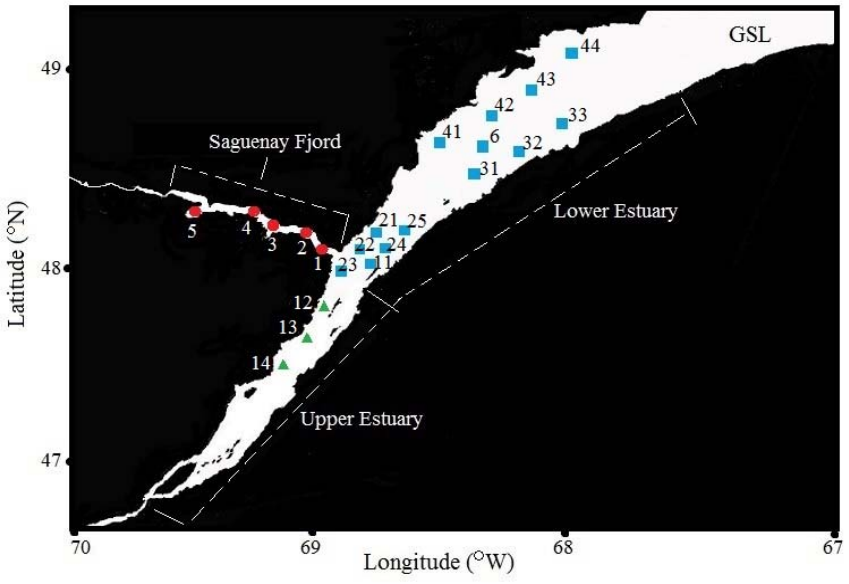

fig. 1

Biogeosciences Discuss., https://doi.org/10.5194/bg-2017-159
Manuscript under review for journal Biogeosciences
Discussion started: 1 June 2017

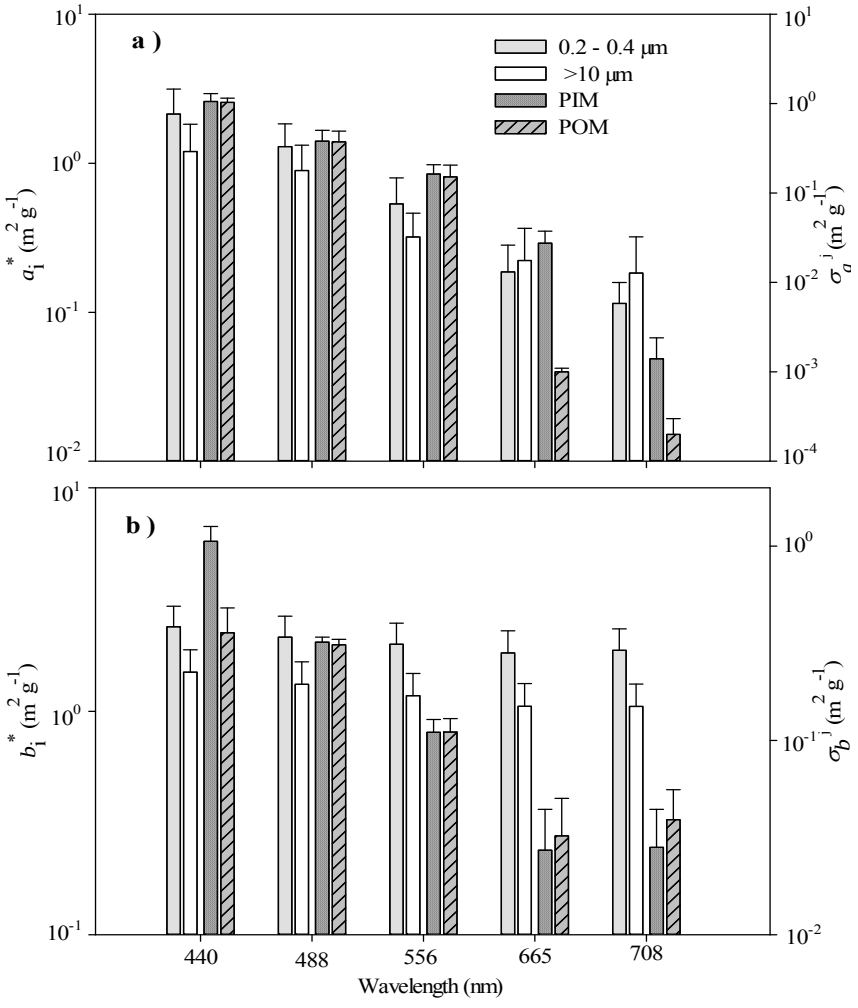

fig. 2

Biogeosciences Discuss., https://doi.org/10.5194/bg-2017-159
Manuscript under review for journal Biogeosciences
Discussion started: 1 June 2017

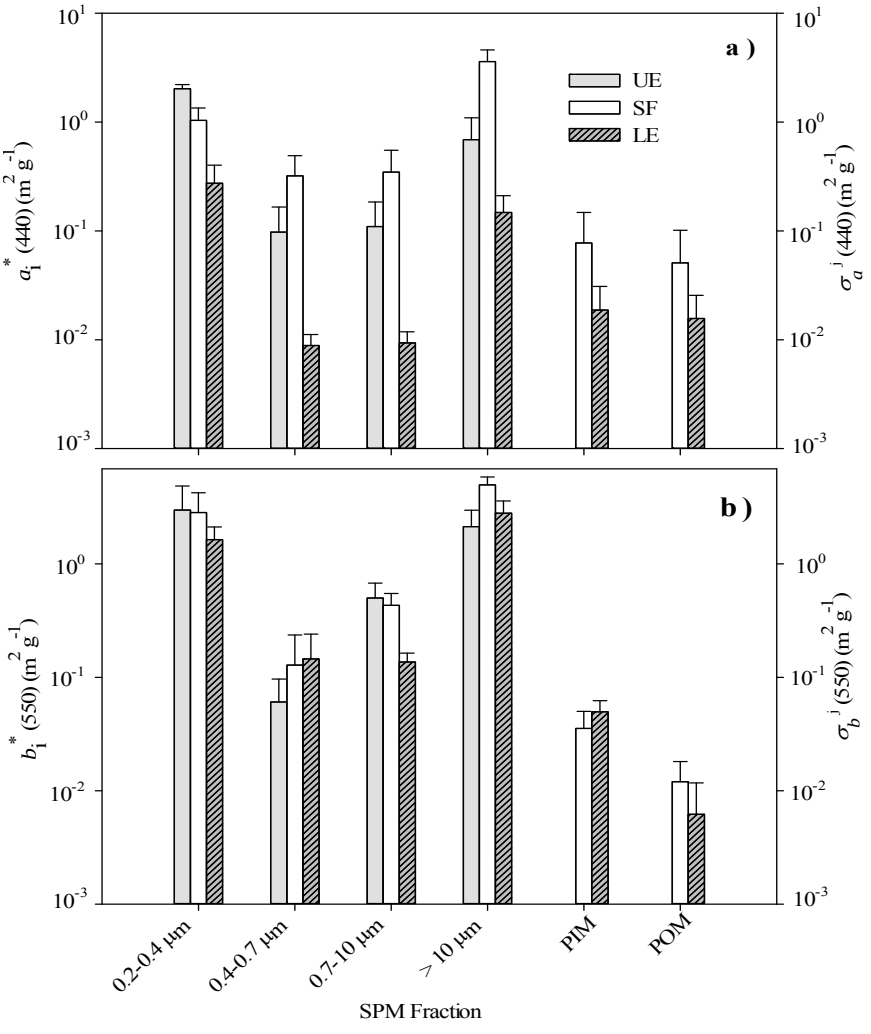

5 fig. 3